

CHEMOGRAPHIC EXPLORATION OF THE MILARITE-TYPE STRUCTURE

OLIVIER C. GAGNÉ[§] AND FRANK C. HAWTHORNE[§]

Department of Geological Sciences, University of Manitoba, 125 Dysart Road, Winnipeg, Manitoba, R3T 2N2, Canada

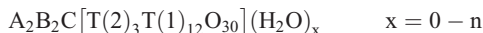
ABSTRACT

The milarite structure-type has an uncommonly large number of distinct mineral species (23 at present). Here we explore this structure type from the point of view of possible root-charge arrangements and endmember compositions. Enumeration shows that there are 34 distinct root-charge arrangements with $\text{Si} = 12$ *apfu* and 39 distinct root-charge arrangements with $\text{Si} = 8\text{--}11$ *apfu*. *A priori* bond-valence calculations for all root-charge arrangements allows evaluation of lattice-induced strain as a function of chemical composition for all arrangements for which the detailed atomic arrangement has been refined. Analysis of localized strain indicates that the *B* site has the highest amount of strain in the structure, and in accord with this finding, milarite-group minerals with vacancies at the *B* site are more common than milarite-group minerals with fully occupied *B* sites. The *a priori* bond-valence calculations suggest that many other compositions are possible for the milarite structure-type. Examination of synthesis results reveals 20 synthetic compounds with the milarite-type structure that have distinct (dominant) endmember compositions. Examination of ~350 chemical analyses from the literature reveals 29 distinct endmember compositions, six of which deserve to be described as new mineral species. Two additional analyses could lead to new minerals, but require confirmation of site populations by structure refinement.

Keywords: milarite, crystal structure, chemographic exploration, bond-valence, lattice strain.

INTRODUCTION

Milarite, ideally $\text{K}_2\text{Ca}[\text{AlBe}_2\text{Si}_{12}\text{O}_{30}](\text{H}_2\text{O})$, was first described by Kuschel (1877) from Val Giuf, Tavetsch, Grischun, Switzerland, and a relatively large number of minerals are now known that have this specific structural arrangement. The general formula of the minerals of the milarite group (Forbes *et al.* 1972) may be written as



where the cation species corresponding to the letters of the formula for all endmember compositions of approved minerals are listed in Table 1. Note that groups of cations are listed as regular letters, whereas crystallographic sites are written in italic letters. As is apparent from Table 1, the milarite structure is extremely flexible with regard to its constituent cations, and a considerable number of minerals (Table 2) and synthetic compounds adopt this basic atomic arrangement. The value of *n*, the maximum amount of H_2O in the structure, is not well-characterized, and we will examine this issue here.

DESCRIPTION OF THE MILARITE STRUCTURE-TYPE

Milarite is hexagonal, space group *P6/mcc*, $a \approx 10.40$, $c \approx 13.80$ Å, although various compositions can show anomalous biaxial behavior (*e.g.*, Goldman & Rossman 1978, Janeczek 1986). Milarite was originally considered a (double-)ring silicate, the structure of which was related to that of beryl by melding two beryl $[\text{Si}_6\text{O}_{18}]$ rings through their apical vertices to form an $[\text{Si}_{12}\text{O}_{30}]$ double-ring. However, inclusion of other types of tetrahedra into such structural considerations (Zoltai 1960, Liebau 1985) led to the consideration of beryl and milarite as framework berylllo-alumino-silicates, and Hawthorne & Smith (1986, 1988) showed that the structures of both beryl and milarite can be derived from four-connected three-dimensional nets in a similar fashion to other framework alumino-silicates. Thus the milarite structure is now considered as a framework structure. Cation-coordination polyhedra are identified by the name of the central cation site, *e.g.*, the *T*(1) tetrahedron.

[§] Corresponding author e-mail address: frank_hawthorne@umanitoba.ca

TABLE 1. SITES AND SITE OCCUPANCIES IN THE MILARITE-GROUP MINERALS

Site	Equipoint	C.N.	Occupancy
T(1)	24m	4	Si, Al
T(2)	6f	4	Li, Be, B, Mg, Al, Si, Mn ²⁺ , Zn
A	4c	6	Al, Fe ³⁺ , Sn ⁴⁺ , Mg, Zr, Fe ²⁺ , Ca, Na, Y, Sc
B	4d	9	Na, H ₂ O, □, K
C	2a	12	K, Na, Ba, □
D	2b	18	□

The T(1) tetrahedron

This tetrahedron shares O anions with two other T(1) tetrahedra to form a six-membered ring with the tetrahedra all pointing in the same direction (as

in beryl), and the apical anions of this ring are shared with T(1) tetrahedra of another ring to form an [Si₁₂O₃₀] double six-membered ring (Figs. 1 and 2). The T(1) tetrahedron thus shares three anions with adjacent T(1) tetrahedra and one anion with a T(2) tetrahedron that links the [Si₁₂O₃₀] clusters into a framework (Figs. 1 and 2). The <T(1)–O> distances in refined milarite structures show little variation (± 0.002 Å in the data of Černý *et al.* 1980 and Hawthorne *et al.* 1991). However, the corresponding chemical data show a well-developed positive correlation between the Si content and the Be/(Be + Al) ratio, indicating slight replacement of Si by Al (maximum = 0.1 Al *apfu*) that is insufficient to significantly affect the size of the T(1) tetrahedron.

TABLE 2. CURRENT MINERALS OF THE MILARITE GROUP: ENDMEMBER COMPOSITIONS, SITE OCCUPANCIES, AND ROOT-CHARGE ARRANGEMENTS

Name	A ₂	B ₂	C	T(2) ₃	T(1) ₁₂	O ₃₀	Root-charge arrangement	Refs.
Agakhanovite-(Y)	YCa	□ ₂	K	Be ₃	Si ₁₂	O ₃₀	[21]	(1)
Almarudite	Mn ₂	□ ₂	K	Be ₂ Al	Si ₁₂	O ₃₀	[10]	(2)
Armenite	Ca ₂	□ ₂	Ba	Al ₃	(Si ₉ Al ₃)	O ₃₀	{8}	(3)
Berezanskite	Ti ₂	□ ₂	K	Li ₃	Si ₁₂	O ₃₀	[29]	(4)
Brannockite	Sn ₂	□ ₂	K	Li ₃	Si ₁₂	O ₃₀	[29]	(5)
Chayesite	Mg ₂	□ ₂	K	Mg ₂ Fe ³⁺	Si ₁₂	O ₃₀	[10]	(6)
Darapiosite	Mn ₂	Na ₂	K	LiZn ₂	Si ₁₂	O ₃₀	[24]	(7)
Dusmatovite	Mn ₂	K□	K	Zn ₃	Si ₁₂	O ₃₀	[17]	(8)
Eifelite	MgNa	Na ₂	K	Mg ₃	Si ₁₂	O ₃₀	[18]	(9)
Friedrichbeckeite	Mg ₂	Na□	K	Be ₃	Si ₁₂	O ₃₀	[17]	(10)
Klöchite	Fe ²⁺ Fe ³⁺	□ ₂	K	Zn ₃	Si ₁₂	O ₃₀	[21]	(11)
Merrihueite	Fe ²⁺ ₂	Na□	K	Fe ²⁺ ₃	Si ₁₂	O ₃₀	[17]	(12)
Milarite	Ca ₂	□ ₂	K	Be ₂ Al	Si ₁₂	O ₃₀	[10]	(13)
Oftedalite	ScCa	□ ₂	K	Be ₃	Si ₁₂	O ₃₀	[21]	(14)
Osumilite	Fe ²⁺ ₂	□ ₂	K	Al ₃	Si ₁₀ Al ₂	O ₃₀	{6}	(15)
Osumilite-(Mg)	Mg ₂	□ ₂	K	Al ₃	Si ₁₀ Al ₂	O ₃₀	{6}	(16)
Poudretteite	Na ₂	□ ₂	K	B ₃	Si ₁₂	O ₃₀	[2]	(17)
Roedderite	Mg ₂	Na□	K	Mg ₃	Si ₁₂	O ₃₀	[17]	(18)
Shibkovite	Ca ₂	K□	K	Zn ₃	Si ₁₂	O ₃₀	[17]	(19)
Sogdianite	Zr ₂	□ ₂	K	Li ₃	Si ₁₂	O ₃₀	[29]	(20)
Sugilite	Fe ³⁺ ₂	Na ₂	K	Li ₃	Si ₁₂	O ₃₀	[32]	(21)
Trattnerite	Fe ³⁺ ₂	□ ₂	□	Mg ₃	Si ₁₂	O ₃₀	[20]	(22)
Yagiite	Mg ₂	□ ₂	Na	Al ₃	Si ₁₀ Al ₂	O ₃₀	{6}	(23)

References: (1) Hawthorne *et al.* (2014), Černý *et al.* (1991); (2) Mihajlović *et al.* (2004); (3) Neumann (1941); (4) Pautov & Agakhanov (1997), Hawthorne *et al.* (2015); (5) White *et al.* (1973), Armbruster & Oberhänsli (1988b); (6) Velde *et al.* (1989); (7) Semenov *et al.* (1975), Ferraris *et al.* (1999); (8) Pautov *et al.* (1996), Sokolova & Pautov (1995); (9) Abraham *et al.* (1983); (10) Lengauer *et al.* (2009); (11) Bojar *et al.* (2011); (12) Dodd *et al.* (1965); (13) Hawthorne *et al.* (1991); (14) Cooper *et al.* (2006); (15) Miyashiro (1956), Armbruster & Oberhänsli (1988a); (16) Chukanov *et al.* (2011), Balassone *et al.* (2008); (17) Grice *et al.* (1987); (18) Fuchs *et al.* (1966), Hentschel *et al.* (1980), Armbruster (1989); (19) Pautov *et al.* (1998), Sokolova *et al.* (1999); (20) Dusmatov *et al.* (1968), Cooper *et al.* (1999), Sokolova *et al.* (2000); (21) Murakami *et al.* (1976), Kato *et al.* (1976); (22) Postl *et al.* (2004); (23) Bunch & Fuchs (1969).

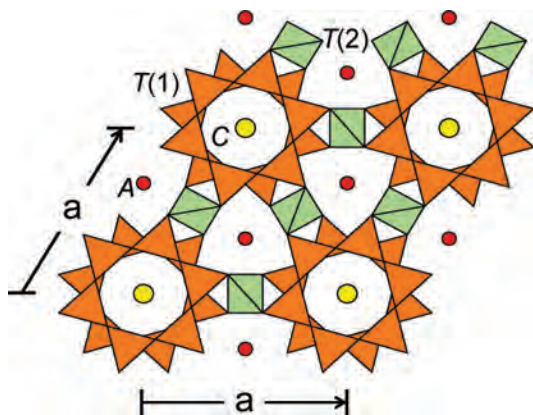


FIG. 1. The crystal structure of milarite projected down the *c* axis. *T*(1) tetrahedra: orange; *T*(2) tetrahedra: green; *A* site: small red circle; *C* site: yellow circle.

The *T*(2) tetrahedron

The *T*(2) tetrahedron shares four anions with adjacent *T*(1) tetrahedra and links the $[\text{Si}_{12}\text{O}_{30}]$ clusters into a framework (Figs. 1 and 2). It also shares two edges with adjacent *A* octahedra. Refinement of several milarite samples of differing chemical compositions (Hawthorne *et al.* 1991) has shown that this site is occupied by variable amounts of Be and Al, and the $\langle T(2)\text{--O} \rangle$ distance varies linearly as a function of $\text{Be}/(\text{Be} + \text{Al})$ ratio.

The *A* octahedron

The *A* octahedron lies on the threefold axis between the $[\text{Si}_{12}\text{O}_{30}]$ clusters, sharing corners with the *T*(1) tetrahedra and further strengthening the linkage of the framework of tetrahedra. It also shares edges with three flanking *T*(2) tetrahedra (Fig. 1). This site is ideally completely occupied by Ca in milarite itself. However, the *A* cation generally shows extremely anisotropic displacement parameters, with the long axis of the ellipsoid oriented along the *c* axis; this has been modelled by a “split site” (Kimata & Hawthorne 1989, Armbruster *et al.* 1989), and the amount of splitting correlates with the $\text{Be}/(\text{Be} + \text{Al})$ ratio of the structure in milarite itself.

The *B* polyhedron

The *B* site lies on the threefold axis, between the $[\text{Si}_{12}\text{O}_{30}]$ clusters, and directly above and below the *A* octahedron (Fig. 2), surrounded by nine O atoms. The ideal *B* site occurs at $z = 0$ and has three O neighbors at ~ 2.78 Å and six O neighbors at ~ 3.30 Å. The *B*-site constituents show very anisotropic displacement

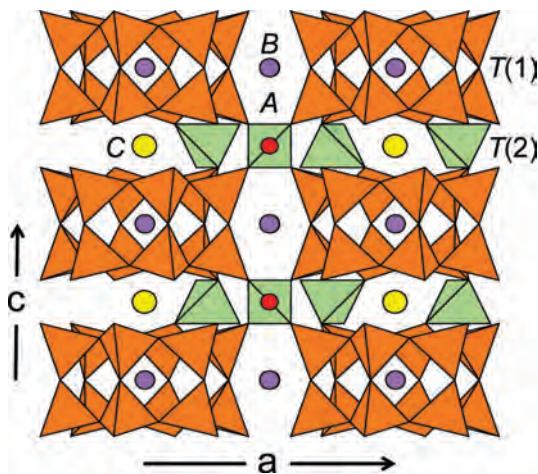


FIG. 2. The crystal structure of milarite projected orthogonal to the *c* axis. Legend as in Figure 1; *B* site: mauve circle.

behavior (also modelled as a “split-site”). Bakakin *et al.* (1975) and Černý *et al.* (1980) showed that H_2O is an important constituent at the *B* site. However, small amounts of alkali and alkaline-earth cations also occupy this site. Armbruster *et al.* (1989) showed that the split *B* site is occupied by H_2O and that the *B* cations occupy the central *B* site, and went on to suggest that the *A*-site splitting in milarite is the result of $^A\text{Ca}\text{--}^B\text{H}_2\text{O}$ interaction in the *c* direction.

The *C* polyhedron

The *C* site occurs in the channel formed by the $[\text{Si}_{12}\text{O}_{30}]$ clusters that stack along the *c* direction (Figs. 1 and 2) and is coordinated by 12 anions at a distance of ~ 3.02 Å. It is occupied primarily by K in all the milarite-group minerals except armenite, where it is occupied by Ba, and yagiite (Na). The occurrence of Ba at the *C* site in armenite is related to the occurrence of significant Al at the *T*(1) site; the divalent cation at *C* helps satisfy the local bond-valence deficiency at the O(2) anion caused by substitution of trivalent Al for Si at the *T*(1) site.

The *D* site

This site was identified by Forbes *et al.* (1972) and is generally mentioned in discussions of the milarite structure. However, no structure has been reported in which this site is occupied, even by small amounts of any constituent, and we will not consider it further here.

Typical interatomic distances (for sugilite) are shown in Table 3. In combination with Figures 1 and 2, Table 3 provides important stereochemical details

TABLE 3. SELECTED INTERATOMIC DISTANCES (Å) IN SUGILITE*

A–O(3) × 3	1.972(2)	T(1)–O(1)	1.625(1)
A–O(3)' × 3	2.409(1)	T(1)–O(2)	1.620(3)
<A–O>	2.334	T(1)–O(2)"	1.615(2)
		T(1)–O(3)	1.577(1)
B–O(1) × 3	2.420(2)	<T(1)–O>	1.609
B–O(3) × 6	2.733(8)		
<B–O>	2.577	T(2)–O(3) × 4	1.970(2)
C–O(2) × 12	2.944(2)		

* From Armbruster & Oberhänsli (1988b)

when considering chemical substitutions and articulation requirements of the milarite structure.

ENDMEMBERS AND THEIR SIGNIFICANCE

From an algebraic perspective, a chemical system is described in terms of its components. System components are those components required to describe the chemical variability of the system and phase components are those components required to describe the chemical variability in individual phases (Spear 1993). Phase components must be independently variable (Gibbs 1961), *i.e.*, they must be additive, and for minerals, they must be conformable with the structure of that mineral. If we define our system as a specific crystal structure, we may define the components of this system as the smallest set of chemical formulae required to describe the composition of all minerals in the system. The definition, “the smallest set of chemical formulae required to describe the composition of all the phases in the system”, defines the components of the system as its set of endmember compositions, and the set of endmember compositions define the possible composition space occupied by that structure. Endmembers have certain constraints (Hawthorne 2002):

- (1) they must be fixed and conformable with the crystal structure of the mineral;
- (2) they must be neutral (*i.e.*, not carry an electric charge);
- (3) they must be irreducible within the system considered (*i.e.*, they cannot be expressed as two or more simpler compositions that are compatible with the crystal structure of the system).

For the majority of atomic arrangements and chemical compositions, these constraints result in endmember formulae which have a single constituent at each site (*e.g.*, diopside: $\text{CaMgSi}_2\text{O}_6$: M1 = Mg, M2 = Ca, T = Si, O1 = O2 = O3 = O) or group of sites (forsterite: Mg_2SiO_4 : M1 + M2 = Mg, T = Si, O1 = O2 = O3 = O4 = O) in the structure. However, Hawthorne

(2002) showed that some endmembers have two constituents of different valence and in a fixed ratio at one site in their structure (the remaining sites having only one constituent each). A classic example of this is milarite itself (Table 2), in which T(2) = Be_2Al *apfu* (atoms per formula unit) in the endmember formula. Note that, by definition, an endmember can have more than one species at only one site and only two species at that site. If more than one cation or anion is introduced at another site in the structure, or a third species is introduced at a site, the resulting composition is not irreducible and may be resolved into two or more endmember compositions.

Root-charge arrangements

In minerals, homovalent and heterovalent substitutions are very different in character. Homovalent substitutions generally introduce only minor changes in bond valences (due to relaxation of bond lengths), whereas heterovalent substitutions produce major changes in the pattern of bond valences due to the different arrangements of formal charges in the structure. Thus we may identify a set of root-charge arrangements that correspond to the set of endmembers related only by heterovalent substitutions. A set of endmembers related only by homovalent substitutions between themselves will have the same root-charge arrangement.

This difference between homovalent and heterovalent substitutions is embedded in the more recent classification/nomenclature schemes for minerals (*e.g.*, arrojadite, Chopin *et al.* 2006; tourmaline, Henry *et al.* 2011; amphibole, Hawthorne *et al.* 2012), where root compositions are assigned a root name and homovalent analogues are named by adding prefixes or suffixes to the appropriate root name. The idea of root-charge arrangements provides us with a very compact way to evaluate endmember arrangements, as the distinct arrangements with regard to heterovalent substitutions correspond to the distinct arrangements of the corresponding formal charges, and the distinct arrangements with regard to homovalent substitutions correspond to the distinct arrangements of homovalent cations for a specific arrangement of formal charges. We will take this approach to the milarite-type structure and derive its set of endmember compositions.

Root-charge arrangements in the milarite structure-type

Inspection of the (ideal) site-populations listed in Table 2 gives us an idea of what ranges of charges to consider. For the A site, the formal charge varies from 2+ (*e.g.*, A = Na_2 in poudretteite) to 8+ (*e.g.*, A = Ti^{4+}_2

TABLE 4. ROOT-CHARGE ARRANGEMENTS* FOR THE MILARITE STRUCTURE-TYPE WITH Si = 12 *apfu*

Number	Charge at (A + B + C) sites	A ₂	B ₂	C	T(1) ₁₂	T(2) ₃	Charge at [T(1) + T(2)] sites
[1]	3	0 ₂	1 ₂	1 ₁	4 ₁₂	3 ₃	57
[2]	3	1₂	0₂	1₁	4₁₂	3₃	57
[3]	3	0 ₁ 1 ₁	1 ₂	0 ₁	4 ₁₂	3 ₃	57
[4]	3	1 ₂	0 ₁ 1 ₁	0 ₁	4 ₁₂	3 ₃	57
[5]	4	1 ₂	1 ₂	0 ₁	4 ₁₂	3 ₂ 2 ₁	56
[6]	4	2 ₂	0 ₂	0 ₁	4 ₁₂	3 ₂ 2 ₁	56
[7]	4	0 ₂	2 ₂	0 ₁	4 ₁₂	3 ₂ 2 ₁	56
[8]	5	0 ₂	2 ₂	1 ₁	4 ₁₂	3 ₁ 2 ₂	55
[9]	5	1 ₂	1 ₂	1 ₁	4 ₁₂	3 ₁ 2 ₂	55
[10]	5	2₂	0₂	1₁	4₁₂	3₁2₂	55
[11]	6	0 ₂	2 ₂	2 ₁	4 ₁₂	2 ₃	54
[12]	6	2 ₂	0 ₂	2 ₁	4 ₁₂	2 ₃	54
[13]	6	1 ₂	1 ₂	2 ₁	4 ₁₂	2 ₃	54
[14]	6	1 ₂	2 ₂	0 ₁	4 ₁₂	2 ₃	54
[15]	6	2₂	1₂	0₁	4₁₂	2₃	54
[16]	6	0 ₁ 1 ₁	2 ₂	1 ₁	4 ₁₂	2 ₃	54
[17]	6	2₂	0₁1₁	1₁	4₁₂	2₃	54
[18]	6	1₁2₁	1₂	1₁	4₁₂	2₃	54
[19]	6	1 ₂	1 ₁ 2 ₁	1 ₁	4 ₁₂	2 ₃	54
[20]	6	3₂	0₂	0₁	4₁₂	2₃	54
[21]	6	2₁3₁	0₂	1₁	4₁₂	2₃	54
[22]	7	3 ₂	0 ₂	1 ₁	4 ₁₂	2 ₂ 1	53
[23]	7	1 ₂	2 ₂	1 ₁	4 ₁₂	2 ₂ 1	53
[24]	7	2₂	1₂	1₁	4₁₂	2₂1	53
[25]	8	2 ₂	2 ₂	0 ₁	4 ₁₂	2 ₁ 2	52
[26]	8	3₂	1₂	0₁	4₁₂	2₁2	52
[27]	8	4 ₂	0 ₂	0 ₁	4 ₁₂	2 ₁ 2	52
[28]	9	4 ₁ 5 ₁	0 ₂	0 ₁	4 ₁₂	1 ₃	51
[29]	9	4₂	0₂	1₁	4₁₂	1₃	51
[30]	9	4 ₂	0 ₁ 1 ₁	0 ₁	4 ₁₂	1 ₃	51
[31]	9	3 ₁ 4 ₁	1 ₂	0 ₁	4 ₁₂	1 ₃	51
[32]	9	3₂	1₂	1₁	4₁₂	1₃	51
[33]	9	2 ₁ 3 ₁	2 ₂	0 ₁	4 ₁₂	1 ₃	51
[34]	9	2 ₂	2 ₂	1 ₁	4 ₁₂	1 ₃	51

* Those root-charge arrangements shown in bold are the ones that correspond to observed endmember compositions of minerals, potential minerals, and synthetics.

in berezanskite). For the *B* site, the formal charge varies from 0 (e.g., B = □₂ in almarudite) to 2+ (e.g., B = Na₂ in sugilite). For the *C* site, the formal charge varies from 0 (e.g., C = □ in trantnerite) to 2+ (e.g., C = Ba in armenite). For the *T*(2) site, the formal charge varies from 3+ [e.g., T(2) = Li₃ in brannockite] to 9+ [e.g., T(2) = Al₃ in osumilite]. For the *T*(1) site, the formal charge varies from 45+ [e.g., T(1) = Si₉Al₃ in armenite] to 48+ [e.g., T(1) = Si₁₂ in milarite].

Table 4 shows the root-charge arrangements for Si = 12 *apfu*, i.e., T(1) charge = 48+. The arrangements are organized in terms of increasing charge of the A + B + C cations (left-hand column in Tables 4 and 5) and

decreasing charge of the T cations (right-hand column in Table 4). It is immediately apparent on inspection of Table 4 that many root-charge arrangements are not represented by analogous mineral species. There are 34 distinct root-charge arrangements with Si = 12 *apfu*, and nine of these correspond to minerals ([2], [10], [17], [18], [20], [21], [24], [29], [32]). Table 5 shows root-charge arrangements with Si ≠ 12 *apfu* and an aggregate T(1) charge of greater than 44+ (Si₈Al₄) [except for arrangement {25} which has T(1) = 4₆3₆ and was included because it corresponds to one synthetic composition]. Of the 39 arrangements shown, only two correspond to the structures of

TABLE 5. ROOT-CHARGE ARRANGEMENTS* FOR THE MILARITE STRUCTURE-TYPE WITH $\text{Si} \approx 12 \text{ apfu}$

Number	Charge at (A + B + C) sites	A ₂	B ₂	C	T(1) ₁₂	T(2) ₃	Charge at [T(1) + T(2)] sites
{1}	4	1 ₂	1 ₂	0 ₁	4 ₁₁ 3 ₁	3 ₃	56
{2}	4	2₂	0₂	0₁	4₁₁3₁	3₃	56
{3}	4	0 ₂	2 ₂	0 ₁	4 ₁₁ 3 ₁	3 ₃	56
{4}	5	0 ₂	2 ₂	1 ₁	4 ₁₀ 3 ₂	3 ₃	55
{5}	5	1 ₂	1 ₂	1 ₁	4 ₁₀ 3 ₂	3 ₃	55
{6}	5	2₂	0₂	1₁	4₁₀3₂	3₃	55
{7}	6	0 ₂	2 ₂	2 ₁	4 ₉ 3 ₃	3 ₃	54
{8}	6	2₂	0₂	2₁	4₉3₃	3₃	54
{9}	6	1 ₂	1 ₂	2 ₁	4 ₉ 3 ₃	3 ₃	54
{10}	6	1 ₂	2 ₂	0 ₁	4 ₉ 3 ₃	3 ₃	54
{11}	6	2 ₂	1 ₂	0 ₁	4 ₉ 3 ₃	3 ₃	54
{12}	6	3 ₂	0 ₂	0 ₁	4 ₉ 3 ₃	3 ₃	54
{13}	7	3 ₂	0 ₂	1 ₁	4 ₈ 3 ₄	3 ₃	53
{14}	7	1 ₂	2 ₂	1 ₁	4 ₈ 3 ₄	3 ₃	53
{15}	7	2 ₂	1 ₂	1 ₁	4 ₈ 3 ₄	3 ₃	53
{16}	7	3 ₂	0 ₂	1 ₁	4 ₁₁ 3 ₁	2 ₃	53
{17}	7	1 ₂	2 ₂	1 ₁	4 ₁₁ 3 ₁	2 ₃	53
{18}	7	2₂	1₂	1₁	4₁₁3₁	2₃	53
{19}	8	2 ₂	2 ₂	0 ₁	4 ₁₀ 3 ₂	2 ₃	52
{20}	8	3 ₂	1 ₂	0 ₁	4 ₁₀ 3 ₂	2 ₃	52
{21}	8	4 ₂	0 ₂	0 ₁	4 ₁₀ 3 ₂	2 ₃	52
{22}	9	4 ₂	0 ₂	1 ₁	4 ₉ 3 ₃	2 ₃	51
{23}	9	3 ₂	1 ₂	1 ₁	4 ₉ 3 ₃	2 ₃	51
{24}	9	2 ₂	2 ₂	1 ₁	4 ₉ 3 ₃	2 ₃	51
{25}	10	2 ₂	2 ₂	2 ₁	4 ₈ 3 ₄	2 ₃	50
{26}	10	3 ₂	2 ₂	0 ₁	4 ₈ 3 ₄	2 ₃	50
{27}	10	4 ₂	1 ₂	0 ₁	4 ₈ 3 ₄	2 ₃	50
{28}	10	5 ₂	0 ₂	0 ₁	4 ₈ 3 ₄	2 ₃	50
{29}	10	2 ₂	2 ₂	2 ₁	4 ₁₁ 3 ₁	1 ₃	50
{30}	10	3 ₂	2 ₂	0 ₁	4 ₁₁ 3 ₁	1 ₃	50
{31}	10	4 ₂	1 ₂	0 ₁	4 ₁₁ 3 ₁	1 ₃	50
{32}	10	5 ₂	0 ₂	0 ₁	4 ₁₁ 3 ₁	1 ₃	50
{33}	11	5 ₂	0 ₂	1 ₁	4 ₁₀ 3 ₂	1 ₃	49
{34}	11	4 ₂	1 ₂	1 ₁	4 ₁₀ 3 ₂	1 ₃	49
{35}	11	3 ₂	2 ₂	1 ₁	4 ₁₀ 3 ₂	1 ₃	49
{36}	12	5 ₂	1 ₂	0 ₁	4 ₉ 3 ₃	1 ₃	48
{37}	12	4 ₂	2 ₂	0 ₁	4 ₉ 3 ₃	1 ₃	48
{38}	13	5 ₂	1 ₂	1 ₁	4 ₈ 3 ₄	1 ₃	47
{39}	13	4 ₂	2 ₂	1 ₁	4 ₈ 3 ₄	1 ₃	47

* Those root-charge arrangements shown in bold are the ones that correspond to observed endmember compositions of minerals, potential minerals, and synthetics.

milarite-group minerals ({6}, {8}). We are left with a major question: are the other root-charge arrangements not stable, or are there many other milarite structures with chemical compositions analogous to the as yet unrepresented root-charge arrangements that we have not yet discovered or synthesized? We will consider this issue next with regard to the known chemical compositions of the milarite-group minerals.

CHEMICAL COMPOSITIONS OF MILARITE-GROUP MINERALS

A literature review of over 132 publications describing milarite-group minerals and synthetic milarite-group compounds has provided us with ~350 chemical analyses. A list of these publications may be obtained from The Depository of Unpublished

TABLE 6. NEW ENDMEMBER COMPOSITIONS CORRESPONDING TO OBSERVED CHEMICAL COMPOSITIONS OF MILARITE-GROUP MINERALS

Sample number	A_2	B_2	C	$T(2)_3$	$T(1)_{12}$	RCA*	"Name"
PM3	$(\text{Fe}^{2+}, \text{Mg})_2$	$\text{K}\square$	K	$(\text{Fe}^{2+}, \text{Mg})_3$	Si_{12}	[17]	K-merrihueite
KSR	Mg_2	Na_2	K	$(\text{Mg}, \text{Fe}^{2+})_3$	Si_{11}Al	{18}	New RCA
FC1	$(\text{Mg}, \text{Fe}^{2+})\text{Fe}^{3+}$	\square_2	K	Mg_3	Si_{12}	[21]	Mg-klöchite
ALSU	Al_2	Na_2	K	Li_3	Si_{12}	[32]	Al-sugilite
MSO	Mg_2	\square_2	\square	Al_3	Si_{11}Al	{2}	New RCA
FMM	$(\text{Fe}^{2+}, \text{Mg})\text{Fe}^{3+}$	\square_2	K	$(\text{Fe}^{2+}, \text{Mg})_3$	Si_{12}	[21]	Fe-klöchite

* Root-charge arrangement

Data on the MAC website [document Milarite CM54-5_10.3749/canmin.1500088]. There are currently 23 valid mineral species with the milarite structure (Table 2). Among the ~350 analyses, we have identified 29 distinct endmember compositions that are the dominant constituent in one or more chemical analyses, 23 of which correspond to the minerals of Table 2. The remaining six dominant distinct endmember formulae do not correspond to named mineral species. These are listed in Table 6, together with the dominant endmember formulae and the corresponding root-charge arrangement, and the chemical compositions are listed in Table 7. Of course, we have made assumptions with regard to the site populations in the minerals of Table 6; in general, these follow the observed site-populations in Table 2. Where the dominant divalent cations are Mg and Fe^{2+} , there is the potential for order-disorder of these cations over the A and $T(2)$ sites, and without crystal-structure or spectroscopic data, we cannot assign distinct site-populations. In these cases, we have written the site populations as $(\text{Mg}, \text{Fe}^{2+})$ or $(\text{Fe}^{2+}, \text{Mg})$ according to whether Mg or Fe^{2+} is the dominant constituent (e.g., PM3, FC1, and FMM, Table 6).

H_2O content

There is not a lot of reliable information on the H_2O content of milarite-group minerals, in part because of the inherent difficulties of analyzing for H_2O or H, and in part because many of the milarite-group minerals are rare and have only been found in very small quantities. (H_2O) occurs at the B site (Table 1) and hence has a maximum value of 2 *apfu*. Two of the measured values exceed 2 *apfu* and must be wrong unless H_2O occupies another site in the structure, something that has not been confirmed by crystal-structure work. Previous work has suggested that the amount of (H_2O) does not exceed 1 *apfu*. In particular, Hawthorne *et al.* (1991) showed that for the milarite samples of Černý *et al.* (1980), there is a linear relation

between the intensity of the infrared combination mode at $\sim 5200 \text{ cm}^{-1}$ (E perpendicular to c) and the (H_2O) content, and the maximum amount of (H_2O) in this correlation is 1.12 *apfu*. Inspection of Figure 3 shows four values significantly exceeding this value, suggesting that the (H_2O) content of the milarite structure does go up to 2 *apfu*. The crystal-chemical role of (H_2O) in the milarite structure is not clear. Hawthorne *et al.* (1991) showed that the two-fold rotation axis of the (H_2O) group is parallel to the c axis, and the relatively short A–B distance in some milarites (e.g., Černý *et al.* 1980) suggests that there could possibly be an interaction between the A -site cation and (H_2O) at the B site. On the other hand, many milarite-group minerals are anhydrous, suggesting that (H_2O) does not bond directly to any cation and hence belongs to the *occluded (H_2O)* category of Hawthorne (1992). This situation remains to be resolved in a convincing manner.

Potential new mineral species

There are other analyses in the literature for which the site assignments are ambiguous, and new minerals are possible if the associated site-populations can be derived experimentally. These are listed in Tables 8 and 9. The compositions have the root-charge arrangement of merrihueite and roedderite (Table 2). In endmember roedderite, $A_2 = \text{Mg}_2$ and $T(2)_3 = \text{Mg}_3$, and in merrihueite, $A_2 = \text{Fe}^{2+}_2$ and $T(2)_3 = \text{Fe}^{2+}_3$. The possible variation in formulae along the solid solution roedderite-merrihueite is shown in Figure 4. Where the A and $T(2)$ sites have the same dominant cation, the species roedderite and merrihueite are distinct. However, where Mg or Fe^{2+} is strongly ordered at A [or $T(2)$], the endmembers $\text{Fe}^{2+}_2\text{Na}\square\text{KMg}_3\text{Si}_{12}\text{O}_{30}$ or $\text{Mg}_2\text{Na}\square\text{KFe}^{2+}_3\text{Si}_{12}\text{O}_{30}$ can become dominant and compositions in the unnamed areas of Figure 4 then require distinct mineral names.

TABLE 7. CHEMICAL FORMULAE CONSISTENT WITH NEW DOMINANT ENDMEMBER COMPOSITIONS

	PM3	KSR	FC1	AISU	MSO	FMM
SiO ₂ (wt.%)	62.12	68.00	68.98	71.50	63.51	61.80
TiO ₂	0.00	0.00	0.08	0.00	—	—
Al ₂ O ₃	0.05	2.50	0.15	3.59	20.88	0.02
Cr ₂ O ₃	0.02	0.00	0.00	0.00	—	—
Fe ₂ O ₃	0.00	0.00	6.70	5.48	—	—
Mn ₂ O ₃	0.00	0.00	0.00	3.19	—	—
FeO	25.31	0.40	5.29	0.00	6.41	23.70
MnO	0.00	0.00	0.23	0.00	—	0.50
MgO	4.18	19.00	12.85	0.00	4.53	4.40
BeO	—	—	—	—	—	—
CaO	0.06	0.00	0.00	0.00	0.15	0.30
Li ₂ O	0.00	0.00	0.00	3.67	—	—
Na ₂ O	0.49	5.30	0.43	6.09	0.35	2.00
K ₂ O	6.66	3.80	4.50	0.75	4.04	3.80
TOTAL	98.89	99.00	99.21	99.24	99.87	96.70
Si (<i>apfu</i>)	11.91	11.55	11.96	12.19	10.63	12.00
Al	0.01	0.45	0.03	—	1.37	—
ΣT(1)	11.92	12.05	11.99	12.19	12.00	12.00
Li	—	—	—	2.52	—	—
Be	—	—	—	—	—	—
Mg+Fe ²⁺	—	2.97	3.00	—	0.25	—
Fe ²⁺ +Mg	3.00	—	—	—	—	3.00
Al	—	0.03	—	0.48	2.75	—
ΣT(2)	3.00	3.00	3.00	3.00	3.00	3.00
K	1.00	0.82	1.00	1.08	0.06	0.47
□	—	0.18	—	—	0.94	Na 0.36
ΣC	1.00	1.00	1.00	1.08	1.00	0.83
Na	0.18	1.75	0.15	2.01	0.10	—
K	0.63	—	—	—	—	—
□	1.19	0.25	1.85	—	1.90	2.00
ΣB	2.00	2.00	2.00	2.01	2.00	2.00
Mg + Fe ²⁺	—	1.84	0.32	—	1.74	1.27
Fe ²⁺ + Mg	2.25	0.06	0.77	—	—	—
Mn ²⁺	—	—	0.03	—	—	0.08
Al	—	—	—	—	—	—
Ca	—	—	—	0.72	0.02	0.06
Fe ³⁺	—	—	0.87	0.71	—	0.85
Mn ³⁺	—	—	—	0.41	—	—
Y + REE	—	—	—	0.16	—	—
□	—	0.10	—	—	0.26	—
ΣA	2.25	2.00	2.00	2.00	2.00	2.26
References	(1)	(2)	(3)	(4)	(5)	(6)

(1) Wood & Holmberg (1994); (2) Krot & Wasson (1994); (3) Alietti *et al.* (1994); (4) Taggart *et al.* (1994); (5) Bogdanova *et al.* (1980); (6) Dodd *et al.* (1965).

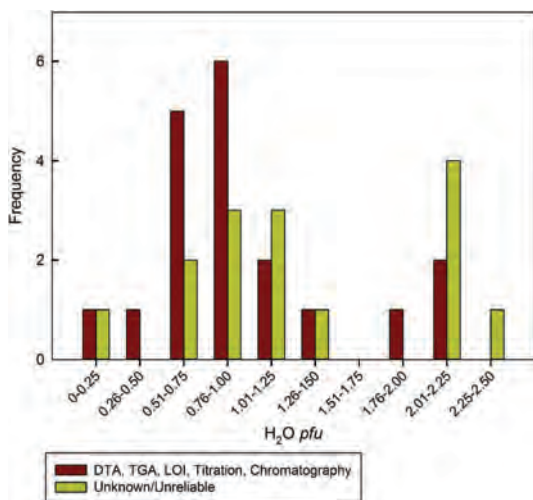


FIG. 3. A histogram of the H₂O content (in molecules *pfu*) in milarite-group minerals taken from the literature. Measured values are shown in red, estimated values are shown in green.

SYNTHETIC COMPOUNDS WITH THE MILARITE-TYPE STRUCTURE

There are 20 synthetic compounds with the milarite-type structure that have distinct (dominant) endmember compositions. Those for which the crystal structure and site populations have been determined are listed in Table 10, and those for which the formulae are assumed from the starting compositions of the experimental charges are listed in Table 11. In Table 10, “Mg-merrihueite”, “Zn-milarite”, and “Mn-milarite” are the names assigned in the original studies (and hence are retained here). “Mg-merrihueite” and “Zn-milarite” are appropriately named, whereas “Mn-milarite” is actually a Mn-analogue of merrihueite. The compound BaMg₂Al₆Si₉O₃₀ is the Mg analogue of armenite, SrMg₂Al₆Si₉O₃₀ is the Sr-Mg analogue of armenite, and Mg₂Al₄Si₁₁O₃₀ is a new root-charge arrangement: arrangement {2} in Table 5. Most of the remaining silicate milarite compounds have root-charge arrangements [17] and [26] (Table 10). The

compound Na₂Mg₃Cu₂Si₁₂O₃₀ is unusual in having root-charge arrangement [15], which inspection of Tables 2 and 6 shows is the first occurrence of this arrangement. The compound Na_{2.90}Al₅[Al_{6.16}Ge_{5.84}O_{29.87}] also has a novel root-charge arrangement: {25} (Table 5).

THE RELATIVE STABILITY OF ROOT-CHARGE ARRANGEMENTS WITH THE MILARITE STRUCTURE

There are 73 distinct root-charge arrangements with the milarite structure, as listed in Tables 4 and 5, and 15 of these occur in minerals and synthetic compounds (Table 12). The obvious question arises: Can all these root-charge arrangements lead to stable structures? Certainly some of the arrangements can be thought of as very stable, as they occur in several minerals: for example, arrangement [17] (Table 4) occurs in six minerals, a further three potential minerals, and between eight to 13 synthetic compounds (Table 12), suggesting that it is a particularly stable charge arrangement.

Figure 5 shows the total charge (*pfu*) at the *A* site as a function of total charge at the *T*(2) site in milarite-type structures. Red circles are for Si = 12 *apfu*, green triangles for Si < 12 *apfu*, and the yellow area shows the following charge ranges: $0 \leq A_2 \leq 10$, $3 \leq T(2)_3 \leq 9$. The red dotted lines bound the range where Si ≤ 12 *apfu*. The region to the bottom left of the figure is forbidden, as there is insufficient charge at the *B* and *C* sites to produce electroneutrality, and the lower red line provides a lower bound for the observed root-charge arrangements. The corresponding upper limit for root-charge arrangements with Si = 12 *apfu* (the upper red line) provides an upper bound for structures with Si = 12 *apfu*. Above this line, all root-charge arrangements (and observed structures) have Si < 12 *apfu*. In principle, the aggregate charge at *T*(2)₃ could be 12 (or even higher if ^{*T*(1)}Si < 12 *apfu*); however, a completely silicate milarite structure, ^{*A*}0₂^{*B*}0₂^{*C*}0₁^{*T*(2)}Si₃^{*T*(1)}Si₁₂O₃₀, seems unlikely because of the number of unoccupied large cavities in the structure.

We may examine aspects of observed and algebraically possible root-charge arrangements using *a priori* bond-valence calculations; we will do this next.

TABLE 8. COMPOSITIONS WHICH MAY LEAD TO NEW ENDMEMBER COMPOSITIONS IN THE MILARITE-GROUP MINERALS

Sample number	<i>A</i> ₂	<i>B</i> ₂	<i>C</i>	<i>T</i> (2) ₃	<i>T</i> (1) ₁₂	RCA*	“Name”
MM	(Fe ²⁺ ,Mg) ₂	Na□	K	(Fe ²⁺ ,Mg) ₃	Si ₁₂	[17]	Mg-merrihueite ?
FR	(Mg,Fe ²⁺) ₂	Na□	K	(Mg,Fe ²⁺) ₃	Si ₁₂	[17]	Fe-roedderite ?

* Root-charge arrangement (from Tables 3 and 4).

TABLE 9. CHEMICAL FORMULAE CORRESPONDING TO THE “ENDMEMBERS” OF TABLE 8

	MM	FR
SiO ₂ (wt.%)	65.70	67.20
TiO ₂	0.00	0.00
Al ₂ O ₃	0.08	0.09
Cr ₂ O ₃	0.03	0.00
Fe ₂ O ₃	0.00	0.00
Mn ₂ O ₃	0.00	0.00
FeO	20.10	14.40
MnO	0.00	0.19
MgO	7.00	10.60
BeO	—	—
CaO	0.02	0.00
Li ₂ O	—	0.00
Na ₂ O	1.90	3.10
K ₂ O	3.60	4.40
TOTAL	98.43	99.98
Si (<i>apfu</i>)	12.09	11.97
Al	—	0.02
ΣT(1)	12.09	11.99
Li	—	—
Be	—	—
Mg + Fe ²⁺	—	3.00
Fe ²⁺ + Mg	2.98	—
Al	0.02	—
ΣT(2)	3.00	3.00
K	0.85	1.00
□	0.15	—
ΣC	1.00	1.00
Na	0.68	1.07
K	—	—
Ca	—	—
□	1.32	0.93
ΣB	2.00	2.00
Mg+Fe ²⁺	—	1.97
Fe ²⁺ +Mg	2.03	—
Mn ²⁺	—	0.03
Al	—	—
Ca	—	—
Fe ³⁺	—	—
Mn ³⁺	—	—
Y+REE	—	—
□	—	—
ΣA	2.03	2.00

References: (1) and (2) Krot & Wasson (1994).

A priori bond-valence calculations

There are two important theorems in bond-valence theory (Brown 2002): (1) the valence-sum rule, and (2) the loop rule. The valence-sum rule states that “the

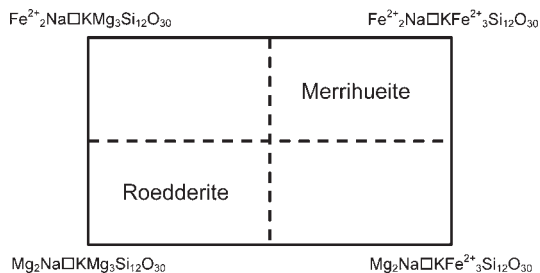


FIG. 4. Possible compositional variation in roedderite–“Mg–merrihueite” structures. In roedderite and “Mg–merrihueite”, the *A* and *T*(2) site-populations are as follows: *A* = Mg₂, *T*(2) = Mg₃ and *A* = Fe²⁺₂, *T*(2) = Fe²⁺₃; however, order of Mg and Fe²⁺ over the *A* and *T*(2) sites can give rise to the following *A* and *T*(2) site-populations: *A* = Mg₂, *T*(2) = Fe²⁺₃ and *A* = Mg₂, *T*(2) = Fe²⁺₃, which correspond to distinct endmember compositions.

sum of the bond valences at each atom is equal to the magnitude of the atomic valence.” The loop rule states that “the sum of the directed bond-valences around any circuit (closed path) of bonds in a structure is zero.” The equations associated with the valence-sum rule and the loop rule result in an exactly determined system with regard to the bond valences; these are called the *a priori* bond-valences, *i.e.*, the bond valences calculated from the formal valences of the ions at each site and the bond-topological characteristics of the structure (Brown 1977, Rutherford 1990). This approach has been used only sparingly, mostly to predict bond lengths of simple structures, based on the solution of the network equations (see below) by extraction and conversion of the *a priori* bond-valences (Brown 1977, Rutherford 1990, Urusov & Orlov 1999, Hawthorne & Sokolova 2008).

An aspect of considerable interest with regard to the milarite structure is the wide range of cations that can occur in this structure type, forming numerous minerals (Table 2). *A priori* bond-valence calculations provide us with an ideal method for examining the control of bond topology on site occupancy in the milarite structure and in the minerals of the milarite group.

The equations involved in the valence-sum rule may be written as follows:

$$\sum s_{ij} = V_i \quad (i = 1 - n) \quad (1)$$

where the summation involves all bonds to the *j* coordinating ions from the central ion *i* for all *n* ions in the structure.

The equations for the loop rule may be written as follows:

TABLE 10. SYNTHETIC MILARITE-LIKE COMPOSITIONS AND CORRESPONDING ENDMEMBERS FOR WHICH CRYSTAL-STRUCTURE REFINEMENTS ARE AVAILABLE

Composition	A_2	B_2	C	$T(2)_3$	$T(1)_{12}$	Anion	RCA*	Ref.
Mg-merrihueite	Mg ₂	K□	K	Mg ₃	Si ₁₂	O ₃₀	[17]	(1)
Zn-milarite	Mn ₂	□ ₂	K	Zn ₂ Fe ³⁺	Si ₁₂	O ₃₀	[10]	(2)
Mn-milarite	Mn ₂	K□	K	Mn ₃	Si ₁₂	O ₃₀	[17]	(3)
BaMg ₂ Al ₆ Si ₉ O ₃₀	Mg ₂	□ ₂	Ba	Al ₃	Si ₉ Al ₃	O ₃₀	{8}	(4)
SrMg ₂ Al ₆ Si ₉ O ₃₀	Mg ₂	□ ₂	Sr	Al ₃	Si ₉ Al ₃	O ₃₀	{8}	(4)
Mg ₂ Al ₄ Si ₁₁ O ₃₀	Mg ₂	□ ₂	□	Al ₃	Si ₁₁ Al	O ₃₀	{2}	(4)
K ₂ Mg ₃ Zn ₂ Si ₁₂ O ₃₀	Mg ₂	K□	K	Zn ₃	Si ₁₂	O ₃₀	[17]	(5)
K ₂ Mg ₃ Fe ₂ Si ₁₂ O ₃₀	Mg ₂	K□	K	Fe ²⁺ ₃	Si ₁₂	O ₃₀	[17]	(5)
RbNaMg ₅ Si ₁₂ O ₃₀	Mg ₂	Na□	Rb	Mg ₃	Si ₁₂	O ₃₀	[17]	(5)
Na ₂ Mg ₅ Si ₁₂ O ₃₀	Mg ₂	Na□	Na	Mg ₃	Si ₁₂	O ₃₀	[17]	(5)
Na ₃ Mg ₄ LiSi ₁₂ O ₃₀	Mg ₂	Na ₂	Na	Mg ₂ Li	Si ₁₂	O ₃₀	[26]	(5)
K ₃ Mg ₄ LiSi ₁₂ O ₃₀	Mg ₂	K ₂	K	Mg ₂ Li	Si ₁₂	O ₃₀	[26]	(5)
Na ₂ Mg ₃ Cu ₂ Si ₁₂ O ₃₀	Mg ₂	Na ₂	□	Cu ₃	Si ₁₂	O ₃₀	[15]	(5)
K ₂ Mg ₃ Cu ₂ Si ₁₂ O ₃₀	Mg ₂	K□	K	Cu ₃	Si ₁₂	O ₃₀	[17]	(5)
Mg ₂ NaNaMg ₃ Si ₁₂ O ₃₀	Mg ₂	Na□	Na	Mg ₃	Si ₁₂	O ₃₀	[17]	(7)

References: (1) Khan *et al.* (1972); (2) Pushcharovskii *et al.* (1972); (3) Sandomirskii *et al.* (1977); (4) Winter *et al.* (1995); (5) Nguyen *et al.* (1980); (7) Artioli *et al.* (2013).

* Root-charge arrangement (from Tables 3 and 4).

$$\sum s_{ij} = 0 \quad (2)$$

where the summation is over the directed bond-valences around any circuit in the digraph (directed graph) of the bond network of the structure.

A priori bond-valences of the milarite structure

A general bond-valence table for the milarite structure is shown in Table 13. The bond valences are represented by the variables a–h. The formal charges of the cations at the various cation sites are written as ^{site}V and the charges of the anions are constrained to equal to their formal valence. This means that there are eight unknowns (the bond valences a–h) and we need eight independent equations to solve for these unknowns.

TABLE 11. SYNTHETIC COMPOSITIONS FOR WHICH THERE ARE NO CRYSTAL-STRUCTURE REFINEMENTS

Number	A_2	B_2	C	$T(2)_3$	$T(1)_{12}$	RCA*	Ref.
(1)	Mg ₂	Na ₂ □	Zn ₃	Si ₁₂	Si ₁₂	[15] or [17]	(1)
(3)	Mg ₂	Na ₂ □	Fe ²⁺ ₃	Si ₁₂	Si ₁₂	[15] or [17]	(1)
(5)	Mg ₂	NaRb□	Fe ²⁺ ₃	Si ₁₂	Si ₁₂	[15] or [17]	(1)
(13)	Mg ₂	NaK□	Cu ₃	Si ₁₂	Si ₁₂	[15] or [17]	(1)
(14)	Mg ₂	NaRb□	Cu ₃	Si ₁₂	Si ₁₂	[15] or [17]	(1)

* Root-charge arrangement; Reference: (1) Choisnet *et al.* (1981)

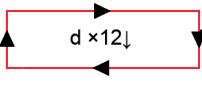
The valence-sum rule for the cations gives us the following equations:

$$\begin{aligned} 6a &= {}^A V \\ 3b + 6c &= {}^B V \\ 12d &= {}^C V \\ e + 2f + g &= {}^{T(1)} V \\ 4h &= {}^{T(2)} V \end{aligned} \quad (3)$$

TABLE 12. NUMBERS OF MINERALS AND COMPOUNDS FOR SPECIFIC ROOT-CHARGE ARRANGEMENTS

RCA*	Minerals	Potential minerals	Synthetic compounds
[2]	1	–	–
[10]	3	–	1
[15]	–	–	1 (+ up to 5)
[17]	6	3	8 (+ up to 5)
[18]	1	–	–
[20]	1	–	–
[21]	2	2	–
[24]	1	–	–
[26]	–	–	2
[29]	3	–	–
[32]	1	1	–
{2}	–	1	1
{6}	3	–	–
{8}	1	–	2
{18}	–	1	–

TABLE 13. GENERAL BOND-VALENCE TABLE FOR THE MILARITE STRUCTURE, SHOWING A LOOP IN THE BOND TOPOLOGY

	A_2	B_2	C	$T(1)_{12}$	$T(2)_3$	Σ
O(1)		$b \times 3 \downarrow$		$e \times 2 \rightarrow$		2
O(2)				$f \times 2 \downarrow \times 2 \rightarrow$		2
O(3)	$a \times 6 \downarrow$	$c \times 6 \downarrow$		g	$h \times 4 \downarrow$	2
Σ	A_V	B_V	C_V	$T_1 V$	$T_2 V$	

The valence-sum rule for the anions gives us the following equations:

$$\begin{aligned} b + 2e &= 2 \\ d + 2f &= 2 \\ a + c + g + h &= 2 \end{aligned} \tag{4}$$

These eight equations are constrained by charge balance, and hence there are only seven independent equations. In order to be able to solve for the bond valences, we need an additional equation, linearly independent of the other equations, and this is provided by the loop rule (see above). There are two (equivalent) ways in which we may derive loop equations: (1) by inspection of the crystal structure and (2) *via* the bond-valence table. Figure 6 shows a fragment of the milarite structure. A convenient loop is shown in red in Table 13: $B \rightarrow O(1) \rightarrow T(1) \rightarrow O(3) \rightarrow B$, resulting in the following loop equation:

$$b - e + g - c = 0 \tag{5}$$

This loop may also be constructed in the structure itself (Fig. 6) by tracing out the loop indicated in Table 13.

Note that the sites A , C , and $T(2)$ are each coordinated by only one crystallographically distinct anion and all bonds to each cation are equivalent. This

means that none of these cations can (usefully) participate in loop equations as the directed bond-valences involving each of these cations always sum to zero. On the other hand, their *a priori* bond-valences are calculated directly from the valence-sum equations: $a = A_V/6$; $d = C_V/12$; $h = T(2)V/4$ *vu*.

Solution of the *a priori* bond-valence equations

We may write the system of equations in matrix form as shown below:

$$\mathbf{A} \cdot \mathbf{B} = \mathbf{C}$$

$$\begin{bmatrix} 6 & 0 & 0 & 0 & 0 & 0 & 0 & 0 \\ 0 & 3 & 6 & 0 & 0 & 0 & 0 & 0 \\ 0 & 0 & 0 & 12 & 0 & 0 & 0 & 0 \\ 0 & 0 & 0 & 0 & 1 & 2 & 1 & 0 \\ 0 & 0 & 0 & 0 & 0 & 0 & 0 & 4 \\ 0 & 1 & 0 & 0 & 2 & 0 & 0 & 0 \\ 0 & 0 & 0 & 1 & 0 & 2 & 0 & 0 \\ 1 & 0 & 1 & 0 & 0 & 0 & 1 & 1 \\ 0 & 1 & 1 & 0 & 1 & 0 & 1 & 0 \end{bmatrix} \begin{bmatrix} a \\ b \\ c \\ d \\ e \\ f \\ g \\ h \end{bmatrix} = \begin{bmatrix} 3 \\ 1 \\ 1 \\ 4 \\ 1 \\ 2 \\ 2 \\ 2 \\ 0 \end{bmatrix} \tag{6}$$

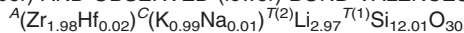
where the \mathbf{A} matrix contains the coefficients of the above equations, the first column vector (\mathbf{B}) contains the *a priori* bond-valences (unknown), and the second

TABLE 14. *A PRIORI* (upper) AND OBSERVED (lower) BOND-VALENCES (*vu*) FOR SUGILITE*:

$A(Mn^{3+}_{0.11}Fe^{3+}_{0.71}Al_{1.16}Na_{0.02})$ $BNa_{1.81}$ $CK_{1.00}$ $T(2)Li_{3.02}$ $T(1)Si_{12.06}$ O_{30}

	A_2	B_2	C	$T(1)_{12}$	$T(2)$	Σ
O(1)		$0.019 \times 3 \downarrow$		$0.991 \times 2 \rightarrow$		2
O(2)			$0.0833 \times 12 \downarrow$	$0.958 \times 2 \downarrow \rightarrow$		2
O(3)	$0.497 \times 6 \downarrow$	$0.141 \times 6 \downarrow$		1.113	$0.252 \times 4 \downarrow$	2
Σ	2.980	0.905	1	4.020	1.007	
O(1)		$0.178 \times 3 \downarrow$		$0.997 \times 2 \rightarrow$		2.172
O(2)			$0.0924 \times 12 \downarrow$	1.010		2.125
				1.023		
O(3)	$0.479 \times 6 \downarrow$	$0.0844 \times 3 \downarrow$ $0.0363 \times 3 \downarrow$		1.128	$0.243 \times 4 \downarrow$	1.971
Σ	2.872	0.896	1.108	4.158	0.973	

* Reference: Armbruster & Oberhänsli (1988b).

TABLE 15. *A PRIORI* (upper) AND OBSERVED (lower) BOND-VALENCES (*vu*) FOR SOGDIANITE*:

	A_2	B_2	C	$T(1)_{12}$	$T(2)$	Σ
O(1)		—		$1.000 \times 2 \rightarrow$		2
O(2)			$0.083 \times 12 \downarrow$	$0.958 \times 2 \downarrow \rightarrow$		2
O(3)	$0.667 \times 6 \downarrow$	—		1.083	$0.248 \times 4 \downarrow$	2
Σ	4	0	1	4.003	0.99	
O(1)		—		$1.044 \times 2 \rightarrow$		2.088
O(2)			$0.0800 \times 12 \downarrow$	1.000		2.100
				1.002		
O(3)	$0.667 \times 6 \downarrow$	—		1.077	$0.252 \times 4 \downarrow$	1.996
Σ	4.004		0.960	4.123	1.008	

* Reference: Sokolova *et al.* (2000)

column vector (**C**) contains the formal charges of the ions at the sites, together with the zero associated with the loop equation. Thus, we may solve this system of equations to obtain the *a priori* bond-valences.

Table 14 shows the results of this calculation for the charge arrangement ${}^A\text{Zr}_{2.98}{}^B\text{Li}_{2.97}{}^C\text{K}_{0.99}{}^{T(1)}\text{Li}_{2.97}{}^{T(2)}\text{Li}_{2.97}\text{O}_{30}$ corresponding to sugilite: $\text{Fe}^{3+}_2\text{Na}_2\text{KSi}_{12}\text{Li}_3\text{O}_{30}$, together with the bond valences calculated from the structure of Armbruster & Oberhänsli (1988b) and the bond-valence parameters of Gagné & Hawthorne (2015). By-and-large, the *a priori* bond-valence calculations reproduce the observed bond-valences quite closely. The principal deviations between the two occur where there are obvious steric constraints on the adoption of

specific bond-lengths. Thus the major significant difference involves the $B\text{--O}(1)$ bond.

Where the B site is vacant, what are other sources of structural strain in the milarite structure? Let us consider the structure of sogdianite (Cooper *et al.* 1999, Sokolova *et al.* 2000), where the B site is vacant (Table 2). Table 15 shows the calculation for the charge arrangement ${}^A\text{Zr}_{2.98}{}^B\text{Li}_{2.97}{}^C\text{K}_{0.99}{}^{T(1)}\text{Li}_{2.97}{}^{T(2)}\text{Li}_{2.97}\text{O}_{30}$ corresponding to sogdianite: $\text{Zr}_{2.98}\text{KSi}_{12}\text{Li}_3\text{O}_{30}$, together with the bond valences calculated from the structure of Sokolova *et al.* (2000) and the bond-valence parameters of Gagné & Hawthorne (2015). The unoccupied B site in this structure emphasizes the second significant mismatch between the *a priori* and observed bond-valences in the milarite structure, that which occurs at the $T(1)$ site: the bond valences $T(1)\text{--O}(1)$ and $T(1)\text{--O}(2)$ are both too large by approximately 0.04 *vu*. While the origin of these slightly high bond-valences is not clear, we note that this mismatch is a lot less important where the B site is occupied.

A summary of the mismatch between the *a priori* and observed bond-valences for all observed milarite-group minerals is given in Table 16.

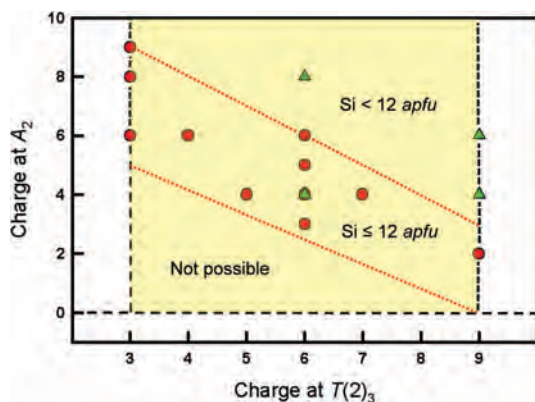


FIG. 5. Total charge (*pfu*) at the A site as a function of total charge at the $T(2)$ site in milarite-type structures; red circles have $\text{Si} = 12$ *apfu*, green triangles have $\text{Si} < 12$ *apfu*, the yellow area shows the following charge ranges: $0 \leq A_2 \leq 10$, $3 \leq T(2)_3 \leq 9$, the red dotted lines bound the range where $\text{Si} \leq 12$ *apfu*.

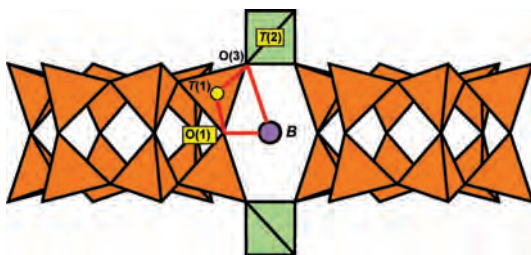


FIG. 6. A fragment of the milarite structure viewed perpendicular to c , showing the loop that is outlined in Table 13 and discussed in the text.

TABLE 16. ABSOLUTE DIFFERENCE BETWEEN A PRIORI BOND-VALENCE AND EXPERIMENTAL BOND-VALENCES (vu) BY BOND

	A-O(3) (1)	A-O(3) (2)	B-O(1)	B-O(3) (1)	B-O(3) (2)	C-O(2)	T(1)-O(1)	T(1)-O(2) (1)	T(1)-O(2) (2)	T(1)-O(3)	T(2)-O(3)
Almarudite	0.005		0.034	0.037	0.042	0.005	0.027	0.083	0.077	0.024	0.014
Darapiosite	0.037		0.088	0.076	0.076	0.002	0.027	0.050	0.034	0.018	0.018
Dusmatovite	0.080		0.081	0.041	0.041	0.002	0.030	0.026	0.042	0.034	0.026
Eifelite	0.084		0.102	0.062	0.110	0.000	0.029	0.047		0.039	0.069
Friedrichbeckeite	0.003		0.075	0.054	0.069	0.009	0.023	0.083	0.080	0.026	0.069
Milarite	0.019	0.087	0.033	0.016	0.018	0.002	0.013	0.058	0.050	0.025	0.029
Oftedalite	0.031					0.002	0.053	0.082	0.066	0.006	0.007
Osumilite	0.016					0.016	0.021	0.050	0.034	0.041	0.015
Osumilite-Mg	0.021					0.015	0.021	0.044	0.028	0.039	0.007
Poudretteite	0.020					0.006	0.045	0.084	0.064	0.027	0.009
Shibkovite	0.018		0.072	0.054	0.054	0.004	0.023	0.047	0.034	0.018	0.017
Sogdianite	0.002					0.003	0.048	0.045	0.043	0.002	0.004
Sugilite	0.017		0.134	0.062	0.100	0.007	0.012	0.074	0.058	0.031	0.008
Average deviation	0.031		0.077	0.057		0.006	0.029	0.055		0.025	0.022

INDUCED STRAIN IN THE MILARITE GROUP

The bond-valence model offers two *a posteriori* checks on the stability of crystal structures: the *Global Instability Index* (GII, Salinas-Sanchez *et al.* 1992) and the *Bond Strain Index* (BSI, Preiser *et al.* 1999). The bond strain index (BSI) is a measure of the lattice-induced strain that causes bonds to violate the network equations (Brown 2002), which results in a mismatch between the *a priori* and experimental bond-valences:

$$\text{BSI} = \left(\frac{\sum_i (w_i (S_{ij} - s_{ij})^2)}{\sum w_i} \right)^{1/2} \quad (7)$$

where S_{ij} is the *a priori* bond-valence, s_{ij} is the corresponding experimental bond-valence, and where the average is taken over all bonds of the bond-topology table. The global instability index (GII) is a complementary measure of the lattice strain, evaluating the difference between the bond-valence sums at the sites of the structure compared to their ideal values:

$$\text{GII} = \left(\frac{\sum_i (w_i (\sum_j s_{ij} - V_i)^2)}{\sum w_i} \right)^{1/2} \quad (8)$$

where s_{ij} are the experimental bond-valences, V_i the valence of the ion, and where the average is taken over all ions of the structure. Brown (2002) states that a value of over 0.2 vu for GII usually indicates a structure too strained to be stable. Table 17 shows the BSI and GII of 14 minerals of the milarite group for which both a reliable chemical analysis and refined crystal-structure is available. The GII varies from 0.06 (osumilite-Mg) to 0.26 vu (eifelite), with an average value of 0.12 vu, whereas the BSI varies from 0.013 (osumilite) to 0.062 vu (eifelite), with an average value of 0.031 vu. These indexes are useful to gauge the relative stability of members of the group. For example, the five highest BSI values involve five minerals with partial or total occupancy of the B site: darapiosite, dusmatovite, eifelite, friedrichbeckeite, and sugilite. These minerals are also on the higher end of the GII values for the group, confirming the relative instability of milarite-group minerals with an occupied B site. There is a correlation coefficient of 0.79 between GII and BSI for the group, meaning that a high BSI does not always equate a high GII or vice versa (*e.g.*, darapiosite). Table 17 also shows that milarite and osumilite have low values of GII and BSI, which could be one of the reasons for their relatively common occurrence compared to that of other minerals of the group.

TABLE 17. GLOBAL INSTABILITY INDEX AND BOND STRAIN INDEX (νu)

	Global Instability Index	Bond Strain Index	Root-charge arrangement
Almarudite	0.13	0.028	[10]
Berezanskite	0.10	0.024	[29]
Darapiosite	0.09	0.040	[24]
Dusmatovite	0.16	0.040	[17]
Eifelite	0.26	0.062	[18]
Friedrichbeckeite	0.13	0.037	[17]
Milarite	0.10	0.019	[10]
Oftedalite	0.13	0.029	[21]
Osumilite	0.07	0.013	{6}
Osumilite-Mg	0.06	0.014	{6}
Poudretteite	0.12	0.026	[2]
Shibkovite	0.09	0.032	[17]
Sogdianite	0.08	0.017	[29]
Sugilite	0.12	0.052	[32]
Average	0.12	0.031	

The B site in the milarite structure

Figure 7 compares the *a priori* bond-valences with the experimental bond-valences for 13 well-refined milarite-group minerals for which reliable chemical analyses are available. Inspection of Figure 7 shows that the maximum deviation from concordance of the *a priori* and experimental bond-valences occurs for the B site, with the B–O(1) bond showing the largest positive deviations and the B–O(3) bond showing the largest negative deviations. In the milarite structure, the B site occupies a cavity within the framework, and the dimensions of that cavity are primarily controlled by the detailed positions of the surrounding polyhedra (Fig. 6). The observed bond-lengths in sugilite are shown in Figure 8a: B–O(1) = 2.42, B–O(3) = 2.73 Å; the ideal bond-lengths corresponding to the *a priori* bond-valences of Table 14 are: B–O(1) = 3.07, B–O(3) = 2.51 Å. These are extremely large differences [up to 0.65 Å for O(1)], and we may understand why the structure cannot adjust to these distances by comparing Figures 8a and 8b. The [Si₁₂O₃₀] units of the milarite structure encapsulate K in [12]-coordination at the C site. The valence-sum rule requires an incident observed bond-valence of 1 νu at the C site, with an *a priori* bond-valence of $1/12 = 0.083 \nu u$ per (symmetry equivalent) bond. This gives a C–O(2) distance of 3.05 Å, close to the 2.99 Å observed in sugilite and ~ 3.05 Å observed in brannockite (Armbruster & Oberhänsli 1988b), sogdianite (Cooper *et al.* 1999, Sokolova *et al.* 2000), and berezanskite (Hawthorne *et al.* 2015). It is apparent that the [Si₁₂O₃₀] groups act as rigid units, buttressed

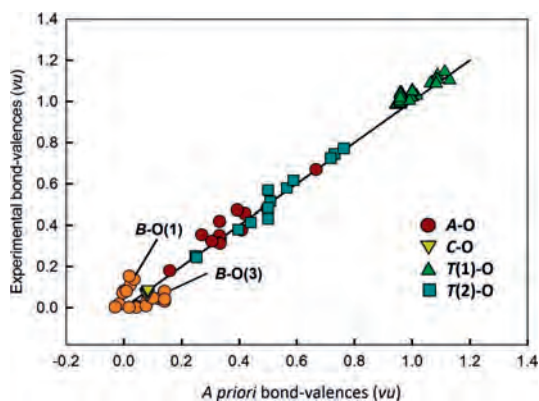


FIG. 7. Comparison of experimental and *a priori* bond-valences for 13 well-refined milarite-group minerals for which reliable chemical analyses are available.

by the central K at the C site. The B–O(1) distance may increase by increasing the distances between the [Si₁₂O₃₀] units in the *a* direction, but this also increases the B–O(3) distance, which is already too long and needs to be shortened, not lengthened. The B–O(3) distance, may be shortened by bringing the [Si₁₂O₃₀] units closer together; however, this will shorten the B–O(1) distance, which needs to be lengthened, and will also further flatten the T(2) tetrahedron, which is already very flat (see Fig. 8b). The only way that B–O(1) may be lengthened and B–O(3) may be shortened is by displacement of the B cation away from the 4d site parallel to the *c* axis. Although this mechanism is not very effective, it is the only one available, and most milarite minerals have the B-site cation “split” up and down the channel direction (*e.g.*, Kimata & Hawthorne 1989).

Compositional implications for milarite-group minerals

The fact that the largest deviations between the *a priori* and observed bond-valences occur at the B site suggests that minerals with an occupied B site will tend to be less stable than those with a vacant B site. In accord with this, of the 23 milarite-group minerals listed in Table 2, 15 have a vacant B site, five have a half-occupied B site, and only three have a fully occupied B site. Moreover, the more common and widespread milarite-group minerals, armenite, milarite, and osumilite, have vacant B sites.

Of the 34 possible root-charge arrangements for the milarite structure with Si = 12 *apfu* that are listed in Table 4, 21 have a fully occupied B site; three of these arrangements ([18], [24], [32]) are known in minerals and two are suspected in synthetic compounds ([15],

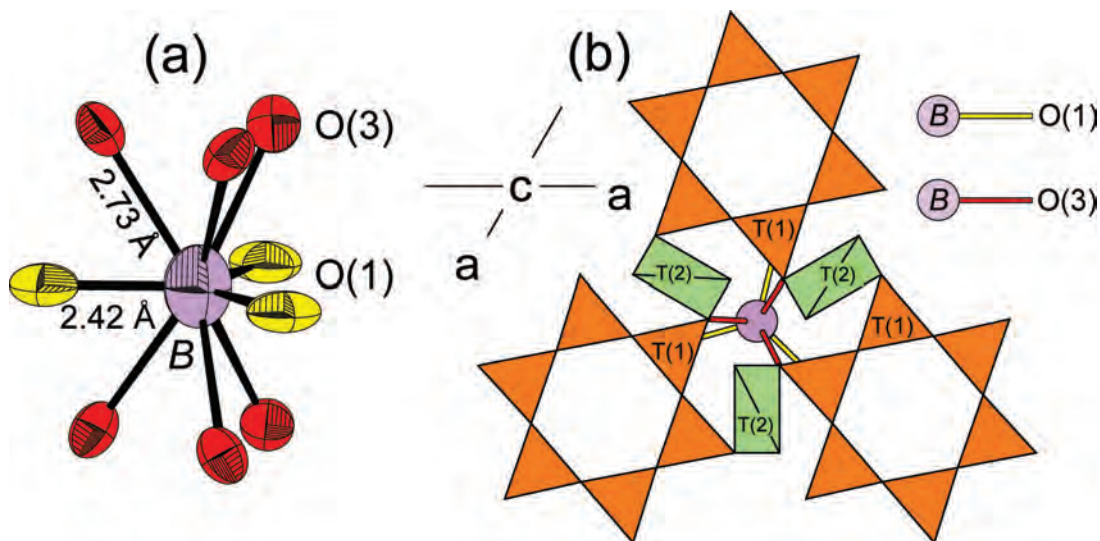


FIG. 8. The coordination around the *B* site in sugilite; (a) ball-and-stick view with the atom-displacements shown; the *B* site has been moved to its ideal position at $z = 0$ to simplify the figure; (b) the polyhedra around the *B* site, with the *B*–O(1) and *B*–O(3) separations shown in yellow and red lines, respectively. Legend as in Figures 1 and 2.

[26]); three have a half-occupied *B* site and one of these arrangements ([17]) is known in minerals; 10 have a vacant *B* site, six of these arrangements ([2], [10], [17], [20], [21], [29]) are known in minerals.

Of the 39 possible root-charge arrangements for the milarite structure with $Si \approx 12$ apfu that are listed in Table 5, 28 have a fully occupied *B* site, and one of these arrangements ({18}) is known in a potential new species identified here; none have a half-occupied *B* site [these arrangements are not possible, as they violate the requirements of an endmember because one site, *T*(1), is already occupied by two cation species]; 11 have a vacant *B* site, two arrangements ({6}, {8}) are known in minerals and one potential new species identified here has another arrangement ({2}).

We note here that most (50) root charge arrangements of the milarite structure have a fully-occupied *B* site, and are therefore less likely to lead to minerals compared to their counterparts. This inventory of distinct root charge arrangements provides many targets for synthesis of materials with the milarite structure, especially with regard to *B* site occupancy.

SUMMARY

- (1) All possible endmember root-charge arrangements for the milarite structure-type have been derived using the criteria of Hawthorne (2002).
- (2) Examination of ~350 chemical analyses from the literature led to the identification of six examples that definitely deserve the status of new minerals; moreover, there are two additional compositions

that may also deserve this status, pending experimental determination of their patterns of cation order.

- (3) Examination of synthesis results reveals 20 synthetic compounds with the milarite-type structure that have distinct (dominant) endmember compositions.
- (4) The inventory of distinct root-charge arrangements provides many targets for synthesis of materials with the milarite structure.
- (5) *A priori* bond-valence calculations on all root-charge arrangements allows evaluation of lattice-induced strain as a function of chemical composition for all arrangements for which the detailed atomic arrangement has been refined.
- (6) Analysis of localized strain indicates that the *B* site has the highest amount of strain in the structure; in accord with this finding, species with a vacant *B* site tend to be more common.
- (7) The inventory of root charge arrangements of the milarite structure shows that out of a total of 74 plausible root charge arrangements, 50 have a fully-occupied *B* site, and in accord with (6), are less likely to lead to minerals than the root charge arrangements with a vacant *B* site.

ACKNOWLEDGMENTS

We thank Yulia Uvarova and Ed Grew for their very helpful comments on this paper. This work was funded by UM Duff Roblin and GETS Fellowships, by

a MAC Foundation Scholarship, and by a PGS-D3 Scholarship from the Natural Sciences and Engineering Research Council of Canada to OCG, by a Canada Research Chair in Crystallography and Mineralogy, by a Natural Sciences and Engineering Research Council of Canada Discovery grant, and by Innovation grants from the Canada Foundation for Innovation to FCH.

REFERENCES

- ABRAHAM, K., GEBERT, W., MEDENBACH, O., SCHREYER, W., & HENTSCHEL, G. (1983) Eifelite, $\text{KNa}_3\text{Mg}_4\text{Si}_{12}\text{O}_{30}$, a new mineral of the osumilite group with octahedral sodium. *Contributions to Mineralogy and Petrology* **82**, 252–258.
- ALIETTI, E., BRIGATTI, M.F., CAPEDEI, S., & POPPI, L. (1994) The roedderite-chayesite series from Spanish lamproites; crystal-chemical characterization. *Mineralogical Magazine* **58**, 655–662.
- ARMBRUSTER, T. (1989) Crystal chemistry of roedderite at 100 and 300 K. *European Journal of Mineralogy* **1**, 715–718.
- ARMBRUSTER, T. & OBERHÄNSLI, R. (1988a) Crystal chemistry of double-ring silicates: Structural, chemical and optical variation in osumilites. *American Mineralogist* **73**, 585–593.
- ARMBRUSTER, T. & OBERHÄNSLI, R. (1988b) Crystal chemistry of double-ring silicates: Structures of sugilite and brannockite. *American Mineralogist* **73**, 594–600.
- ARMBRUSTER, T., BERMANEC, Y., WENGER, M., & OBERHÄNSLI, R. (1989) Crystal chemistry of double-ring silicates: Structure of natural and dehydrated milarite at 100 K. *European Journal of Mineralogy* **1**, 353–362.
- ARTIOLI, G., ANGELINI, I., & NESTOLA, F. (2013) New milarite/ osumilite-type phase formed during ancient glazing of an Egyptian scarab. *Applied Physics A* **110**, 371–377.
- BAKAKIN, V.V., BALKO, V.P., & SOLOVYEV, L.P. (1975) Crystal structures of milarite, armenite, and sogdianite. *Soviet Physics Crystallography* **19**, 460–462.
- BALASSONE, G., MORMONE, A., ROSSI, M., BERNARDI, A., FISCH, M., ARMBRUSTER, T., MALSÝ, A.K., & BERGER, A. (2008) Crystal chemical and structural characterization of an Mg-rich osumilite from Vesuvius volcano (Italy). *European Journal of Mineralogy* **20**, 713–720.
- BOGDANOVA, N.G., TRONEVA, N.V., ZABOROVSKAYA, N.B., SUKHANOV, M.K., & BERKHIN, S.I. (1980) The first find of metamorphic osumilite in the USSR. *Doklady Akademii Nauk SSSR*, **250**(3), 690–693 (in Russian).
- BOJAR, H.-P., WALTER, F., HAUZENBERGER, C., & POSTL, W. (2011) Klöchite, $\text{K}[\square_2(\text{Fe}^{2+}\text{Fe}^{3+})\text{Zn}_3][\text{Si}_{12}\text{O}_{30}]$, a new milarite-type mineral species from the Klöch volcano, Styria, Austria. *Canadian Mineralogist* **49**, 1115–1124.
- BROWN, I.D. (1977) Predicting bond lengths in inorganic crystals. *Acta Crystallographica* **B33**, 1305–1310.
- BROWN, I.D. (2002) *The Chemical Bond in Inorganic Chemistry*. Oxford University Press, Oxford, England.
- BUNCH, T.E. & FUCHS, L.H. (1969) Yagiite, a new sodium-magnesium analogue of osumilite. *American Mineralogist* **54**, 14–18.
- ČERNÝ, P., HAWTHORNE, F.C., & JAROSEWICH, E. (1980) Crystal chemistry of milarite. *Canadian Mineralogist* **18**, 41–57.
- ČERNÝ, P., HAWTHORNE, F.C., JAMBOR, J.L., & GRICE, J.D. (1991) Yttrian milarite. *Canadian Mineralogist* **29**, 533–541.
- CHOISNET, J., CORNET, D., HEMIDY, J.-F., GUYUEN, N., & DAT, Y. (1981) Étude spectroscopique des ions cuivre (II) en coordination tétraédrique dans les silicates synthétiques de type milarite. *Journal of Solid State Chemistry* **40**, 161–169.
- CHOPIN, C., OBERI, R., & CÁMARA, F. (2006) The arrojadite enigma: II. Compositional space, new members, and nomenclature of the group. *American Mineralogist* **91**, 1260–1270.
- CHUKANOV, N.V., PEKOV, I.V., RASTSVETAeva, R.K., AKSENOV, S.M., BELAKOVSKIY, D.I., SCHÜLLER, W., & TERNES, B. (2012) Osumilite-(Mg). IMA 2011-083. CNMNC Newsletter No. 12, February 2012, page 153; *Mineralogical Magazine* **76**, 151–155.
- COOPER, M.A., HAWTHORNE, F.C., & GREW, E.S. (1999) The crystal chemistry of sogdianite, a milarite-group mineral. *American Mineralogist* **84**, 764–768.
- COOPER, M.A., HAWTHORNE, F.C., BALL, N.A., ČERNÝ, P., & KRISTIANSEN, R. (2006) Oftedalite, $(\text{Sc,Ca,Mn}^{2+})_2\text{K}(\text{Be,Al})_3\text{Si}_{12}\text{O}_{30}$, a new member of the milarite group from the Heftefjern pegmatite, Tørdal, Norway: description and crystal structure. *Canadian Mineralogist* **44**, 943–949.
- DODD, R.T., VAN SCHMUS, W.R., & MARVIN, U.B. (1965) Merrihueite, a new alkali ferro-magnesian silicate from the Mezo-Madaras chondrite. *Science* **149**, 972–974.
- DUSMATOV, V.D., EFIMOVA, A.F., KATAEVA, Z.T., KHOROSHILOVA, L.A., & YANULOV, K.P. (1968) Sogdianite, a new mineral. *Doklady Akademii Nauk SSSR* **182**, 1176–1177 (in Russian).
- FERRARIS, G., PRENCIPE, M., PAUTOV, L.A., & SOKOLOVA, E.V. (1999) The crystal structure of darapsite and comparison with Li- and Zn-bearing minerals of the milarite group. *Canadian Mineralogist* **37**, 769–774.
- FORBES, W.C., BAUR, W.H., & KHAN, A.A. (1972) Crystal chemistry of milarite-type minerals. *American Mineralogist* **57**, 463–472.
- FUCHS, L.H., FRONDEL, C., & KLEIN, C., JR. (1966) Roedderite, a new mineral from the Indarch meteorite. *American Mineralogist* **51**, 949–955.
- GAGNÉ, O.C. & HAWTHORNE, F.C. (2015) Comprehensive derivation of bond-valence parameters for ion pairs involving oxygen. *Acta Crystallographica* **B71**, 562–578.

- GIBBS, J.W. (1961) *The Scientific Papers of J. Willard Gibbs, Volume One: Thermodynamics*. Dover Publications, New York City, New York, United States.
- GOLDMAN, D.S. & ROSSMAN, G.R. (1978) The site distribution of iron and anomalous biaxiality in osumilite. *American Mineralogist* **63**, 490–498.
- GRICE, J.D., ERCIT, T.S., VAN VELTHUIZEN, J., & DUNN, P.J. (1987) Poudretteite $\text{KNa}_2\text{B}_3\text{Si}_{12}\text{O}_{30}$, a new member of the osumilite group from Mont Saint-Hilaire, Quebec, and its crystal structure. *Canadian Mineralogist* **25**, 763–766.
- HAWTHORNE, F.C. (1992) The role of OH and H_2O in oxide and oxyalut minerals. *Zeitschrift für Kristallographie* **201**, 183–206.
- HAWTHORNE, F.C. (2002) The use of end-member charge-arrangements in defining new mineral species and heterovalent substitutions in complex minerals. *Canadian Mineralogist* **40**, 699–710.
- HAWTHORNE, F.C. & SMITH, J.V. (1986) Enumeration of 4-connected 3-dimensional nets and classification of framework silicates. 3D nets based on insertion of 2-connected vertices into 3-connected plane nets. *Zeitschrift für Kristallographie* **175**, 15–30.
- HAWTHORNE, F.C. & SMITH, J.V. (1988) Enumeration of 4-connected 3-dimensional nets and classification of framework silicates. Combination of zigzag and saw chains with 6^3 , 3.12_2 , 4.8^2 and $(5^2.8)_2(5.8^2)_1$. *Zeitschrift für Kristallographie* **183**, 213–231.
- HAWTHORNE, F.C. & SOKOLOVA, E. (2008) The crystal chemistry of the scapolite-group minerals: II. The origin of the $I4/m \rightleftharpoons P4_2/n$ phase transition and the non-linear variations in chemical composition. *Canadian Mineralogist* **46**, 1555–1575.
- HAWTHORNE, F.C., KIMATA, M., ČERNÝ, P., BALL, N., ROSSMAN, G.R., & GRICE, J.D. (1991) The crystal chemistry of the milarite-group minerals. *American Mineralogist* **76**, 1836–1856.
- HAWTHORNE, F.C., OBERTE, R., HARLOW, G.E., MARESCH, W.V., MARTIN, R.F., SCHUMACHER, J.C., & WELCH, M.D. (2012) Nomenclature of the amphibole supergroup. *American Mineralogist* **97**, 2031–2048.
- HAWTHORNE, F.C., ABDU, Y.A., BALL, N.A., ČERNÝ, P., & KRISTIANSEN, R. (2014) Agakhanovite-(Y), ideally $(\text{YCa})\square_2\text{KBe}_3\text{Si}_{12}\text{O}_{30}$, a new milarite-group mineral from the Heftefjern Pegmatite, Tørdal, Southern Norway: Description and crystal structure. *American Mineralogist* **99**, 2084–2088.
- HAWTHORNE, F.C., SOKOLOVA, E., PAUTOV, L.A., AGAKHANOV, A.A., & KARPENKO, V.YU. (2016) Refinement of the crystal structure of berezanskite, $\text{Ti}_2\square_2\text{KLi}_3(\text{Si}_{12}\text{O}_{30})$. *Mineralogical Magazine* **18**, 733–737.
- HENRY, D.J., NOVÁK, M., HAWTHORNE, F.C., ERTL, A., DUTROW, B.L., UHER, P., & PEZZOTTA, F. (2011) Nomenclature of the tourmaline super-group minerals. *American Mineralogist* **96**, 895–913.
- HENTSCH, G., ABRAHAM, K., & SCHREYER, W. (1980) First terrestrial occurrence of roedderite in volcanic ejecta of the Eifel, Germany. *Contributions to Mineralogy and Petrology* **73**, 127–130.
- JANECEK, J. (1986) Chemistry, optics, and crystal growth of milarite from Strzegom, Poland. *Mineralogical Magazine* **50**, 271–277.
- KATO, T., MIURA, Y., & MURAKAMI, N. (1976) Crystal structure of sugilite. *Mineralogical Journal* **8**, 183–192.
- KHAN, A.A., BAUR, W.H., & FORBES, W.C. (1972) Synthetic magnesium merrihueite, a dipotassium pentamagnesium dodecasilicate: A tetrahedral magnesian silicate framework crystal structure. *Acta Crystallographica* **B28**, 267–272.
- KIMATA, M. & HAWTHORNE, F.C. (1989) The crystal chemistry of milarite: Two split-site model. *Annual Report of the Institute of Geosciences, University of Tsukuba* **15**, 92–95.
- KROT, A.N. & WASSON, J.T. (1994) Silica-merrihueite/roedderite-bearing chondrules and clasts in ordinary chondrites; new occurrences and possible origin. *Meteoritics* **29**, 707–718.
- KUSCHEL, H. (1877) Mitteilung an Prof. G. Konhard, Milarit. *Neues Jahrbuch für Mineralogie, Geologie und Palaeontologie*, 925–926.
- LENGAUER, C.L., HRAUDA, N., KOLITSCH, U., KRICKL, R., & TILLMANN, E. (2009) Friedrichbeckeite, $\text{K}(\square_{0.5}\text{Na}_{0.5})_2(\text{Mg}_{0.8}\text{Mn}_{0.1}\text{Fe}_{0.1})_2(\text{Be}_{0.6}\text{Mg}_{0.4})_3[\text{Si}_{12}\text{O}_{30}]$, a new milarite type mineral from the Bellerberg volcano, Eifel area, Germany. *Mineralogy and Petrology* **96**, 221–232.
- LIEBAU, F. (1985) *Structural Chemistry of Silicates*. Springer-Verlag, Berlin, Germany.
- MIHAJLOVIĆ, T., LENGAUER, C.L., NTAFLIS, T., KOLITSCH, U., & TILLMANN, E. (2004) Two new minerals, rondorfite, $\text{Ca}_8\text{Mg}[\text{SiO}_4]_4\text{Cl}_2$, and almarudite, $\text{K}(\square, \text{Na})_2(\text{Mn}, \text{Fe}, \text{Mg})_2(\text{Be}, \text{Al})_3[\text{Si}_{12}\text{O}_{30}]$, and a study on iron-rich wadalite, $\text{Ca}_{12}[\text{Al}_8\text{Si}_4\text{Fe}_2\text{O}_{32}]\text{Cl}_6$, from the Bellerberg volcano, Eifel, Germany. *Neues Jahrbuch für Mineralogie - Abhandlungen* **179**, 265–294.
- MIYASHIRO, A. (1956) Osumilite, a new silicate mineral and its crystal structure. *American Mineralogist* **41**, 104–116.
- MURAKAMI, N., KATO, T., MIURA, Y., & KIROTATARI, F. (1976) Sugilite, a new silicate mineral from Iwagi Islet, southwest Japan. *Mineralogical Journal* **8**, 110–121.
- NEUMANN, H. (1941) Armenite, a water-bearing barium-calcium-aluminosilicate. *Norsk Geologisk Tidsskrift* **21**, 19–24.
- NGUYEN, N., CHOISNET, J., & RAVEAU, B. (1980) Silicates synthétiques à structure milarite. *Journal of Solid State Chemistry* **34**, 1–9.
- PAUTOV, L.A. & AGAKHANOV, A.A. (1997) Berezhanskite $\text{KLi}_3\text{Ti}_2\text{Si}_{12}\text{O}_{30}$, a new mineral. *Zapiski Vsesoyuznogo Mineralogicheskogo Obshchestva* **126(4)**, 75–80 (in Russian).

- PAUTOV, L.A., AGAKHANOV, A.A., SOKOLOVA, E.V., & IGNATENKO, K.I. (1996) Dusmatovite, a new mineral of milarite group. *Vestnik Moskovskogo Universiteta, Series 4, Geologicheskaya* **N2**, 54–60 (in Russian).
- PAUTOV, L.A., AGAKHANOV, A.A., & SOKOLOVA, E.V. (1998) Shibkovite, a new mineral of milarite group. *Zapiski Vsesoyuznogo Mineralogicheskogo Obshchestva* **127**(4), 89–94 (in Russian).
- POSTL, W., WALTER, F., ETINGER, K., HAUZENBERGER, C., & BOJAR, H.P. (2004) Trattennerite, $(\text{Fe,Mg})_2(\text{Mg,Fe})_3[\text{Si}_{12}\text{O}_{30}]$, a new mineral of the milarite group: mineral data and crystal structure. *European Journal of Mineralogy* **16**, 375–380.
- PREISER, C., LÖSEL, J., BROWN, I.D., KUNZ, M., & SKWORON, A. (1999) Long-range Coulombic forces and localized bonds. *Acta Crystallographica* **B55**, 698–711.
- PUSHCHAROVSKII, D.YU., BAATARYN, T., POBEDIMSKAYA, E.A., & BELOV, N.V. (1972) The crystal structure of the zinc analogue of milarite. *Soviet Physics Crystallography* **16**, 628–630.
- RUTHERFORD, J.S. (1990) Theoretical prediction of bond-valence networks. *Acta Crystallographica* **B46**, 289–292.
- SALINAS-SANCHEZ, A., GARCIA-MUNOZ, J.L., RODRIGUEZ-CARVAJAL, J., SAEZ-PUCHE, R., & MARTINEZ, J.L. (1992) Structural characterization of R_2BaCuO_5 ($\text{R} = \text{Y, Lu, Yb, Tm, Er, Ho, Dy, Gd, Eu}$ and Sm) oxides by X-ray and neutron-diffraction. *Journal of Solid State Chemistry* **100**, 201–211.
- SANDOMIRSKII, P.A., SIMONOV, M.A., & BELOV, N.V. (1977) Crystal structure of synthetic Mn-milarite $\text{K}_2\text{Mn}_5[\text{Si}_{12}\text{O}_{30}]\cdot\text{H}_2\text{O}$. *Physics Doklady* **22**, 181–183.
- SEMONOV, E.I., DUSMATOV, V.D., KHOMYAKOV, A.P., VORONKOV, A.A., & KAZAKOVA, M. (1975) Darapiosite, a new mineral of the milarite group. *Zapiski Vserossiiskogo Mineralogicheskogo Obshchestva* **104**, 583–584 (in Russian).
- SOKOLOVA, E.V. & PAUTOV, L.A. (1995) Crystal structure of dusmatovite. *Physics Doklady* **40**, 607–610.
- SOKOLOVA, E.V., RYBAKOV, V.B., & PAUTOV, L.A. (1999) Crystal structure of shibkovite. *Doklady Akademii Nauk* **369**(3), 378–380 (in Russian).
- SOKOLOVA, E.V., HAWTHORNE, F.C., & PAUTOV, L.A. (2000) The crystal chemistry of Li-bearing minerals with the milarite-type structure: the crystal structure of end-member sogdianite. *Canadian Mineralogist* **38**, 853–859.
- SPEAR, F.S. (1993) *Metamorphic Phase Equilibria and Pressure-Temperature-Time Paths*. Mineralogical Society of America, Washington D.C., United States, 799 pp.
- TAGGART, J.E., JR., FOORD, E.E., & SHIGLEY, J.E. (1994) Chemical composition and structural formula of mangoan sugilite from the Wessels mine, Republic of South Africa. *Mineralogical Magazine* **58**, 679–681.
- URUSOV, V.S. & ORLOV, I.P. (1999) State-of-art and perspectives of the bond-valence model in inorganic crystal chemistry. *Crystallography Reports* **44**(4), 686–709.
- VELDE, D., MEDENBACH, O., WAGNER, C., & SCHREYER, W. (1989) Chayesite, $\text{K}(\text{Mg,Fe}^{2+})_4\text{Fe}^{3+}[\text{Si}_{12}\text{O}_{30}]$: A new rock-forming silicate of the osumilite group from the Moon Canyon (Utah) lamproite. *American Mineralogist* **74**, 1368–1373.
- WHITE, J.S., JR., AREM, J.E., NELEN, J.A., LEVENS, P.B., & THOMSEN, R.W. (1973) Brannockite, a new tin material. *Mineralogical Record* **4**, 73–76.
- WINTER, W., ARMBRUSTER, T., & LENGAUER, C.L. (1995) Crystal structure refinement of synthetic osumilite-type phases: $\text{BaMg}_2\text{Al}_6\text{Si}_9\text{O}_{30}$, $\text{SrMg}_2\text{Al}_6\text{Si}_9\text{O}_{30}$, and $\text{Mg}_2\text{Al}_4\text{Si}_{11}\text{O}_{30}$. *European Journal of Mineralogy* **7**, 277–286.
- WOOD, J.A. & HOLMBERG, B.B. (1994) Constraints placed on the chondrule-forming process by merrihueite in the mezoemadaras chondrite. *Icarus (Online)* **108**(2), 309–324.
- ZOLTAI, T. (1960) Classification of silicates and other minerals with tetrahedral structures. *American Mineralogist* **45**, 960–973.

Received August 24, 2015. Revised manuscript accepted March 1, 2016.